THE JOURNAL OF BIOLOGICAL CHEMISTRY VOL. 284, NO. 21, pp. 14177–14188, May 22, 2009

Molecular Basis of Catalytic Chamber-assisted Unfolding and Cleavage of Human Insulin by Human Insulin-degrading Enzyme*[S]

Received for publication, January 6, 2009 Published, JBC Papers in Press, March 25, 2009, DOI 10.1074/jbc.M900068200

Marika Manolopoulou[‡1], **Qing Guo**[‡1], **Enrico Malito**[‡], **Alexander B. Schilling**[§], **and Wei-Jen Tang**[‡2]

From the [‡]*Ben-May Department for Cancer Research, University of Chicago, Chicago, Illinois 60637 and the* [§]*Proteomics and Informatics Services Facility, University of Illinois, Chicago, Illinois 60612*

Insulin is a hormone vital for glucose homeostasis, and insulin-degrading enzyme (IDE) plays a key role in its clearance. IDE exhibits a remarkable specificity to degrade insulin without breaking the disulfide bonds that hold the insulin A and B chains together. Using Fourier transform ion cyclotron resonance (FTICR) mass spectrometry to obtain high mass accuracy, and electron capture dissociation (ECD) to selectively break the disulfide bonds in gas phase fragmentation, we determined the cleavage sites and composition of human insulin fragments generated by human IDE. Our time-dependent analysis of IDE-digested insulin fragments reveals that IDE is highly processive in its initial cleavage at the middle of both the insulin A and B chains. This ensures that IDE effectively splits insulin into inactive N- and C-terminal halves without breaking the disulfide bonds. To understand the molecular basis of the recognition and unfolding of insulin by IDE, we determined a 2.6- Å resolution insulin-bound IDE structure. Our structure reveals that IDE forms an enclosed catalytic chamber that completely engulfs and intimately interacts with a partially unfolded insulin molecule. This structure also highlights how the unique size, shape, charge distribution, and exosite of the IDE catalytic chamber contribute to its high affinity (~100 nM) for insulin. In addition, this structure shows how IDE utilizes the interaction of its exosite with the N terminus of the insulin A chain as well as other properties of the catalytic chamber to guide the unfolding of insulin and allowing for the processive cleavages.

IDE[3] is an ~110-kDa zinc metalloprotease that is evolutionarily conserved from bacteria to humans (1, 2). It was first discovered based on its high affinity to bind insulin (~100 nM) and degrade it into pieces (3, 4). Insulin is a 5.8-kDa hormone that plays a central role in glucose homeostasis and the development of diabetes in humans. Consistent with the *in vitro* activity of IDE for insulin degradation, loss-of-function mutations of IDE in rodents result in elevated insulin levels and glucose intolerance (5). In addition, a nucleotide polymorphism of the human IDE gene is linked to type 2 diabetes (6). Later studies showed that IDE can also degrade amyloid-β (Aβ), a peptide vital to the progression of Alzheimer disease (7, 8). Accumulating evidence from rodent models and human genetic analyses also indicate the physiological role of IDE in the clearance of Aβ (5, 9–12).

Despite nearly 60 years of studies on IDE, the molecular basis by which IDE binds, unfolds, and degrades insulin has only begun to be elucidated. Different from ATP-dependent proteases, IDE does not require the additional energy source such as ATP to unfold, bind, and cleave its substrates (4, 13). Insulin consists of the A and B chains that are held together by two inter- and one intra-chain disulfide bonds. Remarkably, IDE does not require disulfide bond isomerase activity to unfold and cleave insulin (4). Thus, IDE needs to overcome the stability created by the disulfide bonds of insulin. Structural analysis reveals that human IDE contains a catalytic chamber formed by the internal cavity of two roughly equally sized ~55-kDa N- and C-terminal halves (IDE-N and IDE-C, respectively) (2). Within this chamber, only one catalytic center exists. However, IDE cleaves insulin at multiple sites on both the insulin A and B chains to completely inactivate this hormone. It remains unclear whether the cleavages of insulin by IDE proceed in a sequential or stochastic manner.

IDE represents an emerging protease family that utilizes an enclosed catalytic chamber to selectively recognize and unfold the substrates for their degradation (1). The volume of the enclosed chamber of IDE (~16,000 Å^3) allows the preferential exclusion of peptides that are greater than ~75 amino acids long. This chamber also has unique electrostatic properties; the internal cavity of IDE-N is predominantly negative, whereas that of IDE-C is positive. Inside the catalytic chamber, IDE has an exosite that is an evolutionarily conserved substrate-binding site ~30 Å away from the catalytic groove. This exosite is used to anchor the N-terminal end of IDE substrates. The unique size, electrostatic potential, and exosite of Ides' catalytic chamber are postulated as key factors for the selective binding and unfolding of IDE substrates (1, 2, 14). In addition, one common feature among the known IDE substrates is their higher pro-

* This work was supported, in whole or in part, by National Institutes of Health Grant GM81539 (to W.-J. T.). This work was also supported by the American Health Assistance Foundation (to E. M.).

The atomic coordinates and structure factors (codes 2WBY and 2WC0) have been deposited in the Protein Data Bank, Research Collaboratory for Structural Bioinformatics, Rutgers University, New Brunswick, NJ (http://www.rcsb.org/).

[S] The on-line version of this article (available at http://www.jbc.org) contains supplemental Table S1 and Figs. S1–S7.

[1] Both authors contributed equally to this work.

[2] To whom correspondence should be addressed: Ben-May Dept. for Cancer Research, 929 East 57th St., University of Chicago, Chicago, Illinois 60637. Tel.: 773-702-4331; Fax: 773-702-4476; E-mail: wtang@uchicago.edu.

[3] The abbreviations used are: IDE, insulin-degrading enzyme; FTICR, Fourier transform ion cyclotron resonance; ECD, electron capture dissociation; MALDI-TOF, matrix-assisted laser desorption ionization time-of-flight; MS, mass spectrometry; MS/MS, tandem mass spectrometry; HPLC, high pressure liquid chromatography; ITC, isothermal titration calorimetry; PDB, Protein Data Bank; Aβ, amyloid-β; ESI, electrospray ionization; IDE-CF, cysteine-free IDE; LC, liquid chromatography.

pensity to form amyloid fibers (8). Amyloidogenic peptides tend to unfold by themselves, which could facilitate their unfolding and subsequent cleavage by IDE. However, the molecular basis of how the catalytic chamber of IDE binds, unfolds, and cleaves insulin into pieces and how the flexibility of this substrate contributes to its cleavage by IDE remain elusive.

IDE is known to cut insulin at multiple sites, and the resulting cleavage products are quite complex (4, 15–18). Here we took advantage of the high mass accuracy of Fourier transform ion cyclotron resonance (FTICR) mass spectrometry and the selective targeting of disulfide bonds by electron capture dissociation (ECD) in our mass spectrometry (MS) analysis to unambiguously identify IDE-degraded fragments of human insulin, as well as the time-dependent production of these fragments. We also present a 2.6- Å insulin-bound IDE structure, revealing extensive shape and charge complementarity of the partially unfolded insulin with the enclosed catalytic chamber and a potential path for the unfolding of insulin. Together, our data elucidate the molecular basis by which IDE engulfs, unfolds, and effectively cleaves insulin into pieces.

EXPERIMENTAL PROCEDURES

IDE Protein Expression and Purification—The construction of cysteine-free IDE mutant (IDE-CF) is as described (19). Wild type human IDE and IDE mutants were expressed in *Escherichia coli* Rosetta (DE3) cells (at 25 °C and 19 h, isopropyl 1-thio-β-D-galactopyranoside induction) and purified by nickel-nitrilotriacetic acid, Source-Q, and Superdex S-200 columns as described previously (2, 14, 19).

Mass Spectrometry—Enzyme reactions were carried out at 37 °C by mixing 5 μl of 1 mg/ml human insulin (RayBiotech) in 20 mM HEPES buffer, pH 7.2, with 5 μl of IDE protein in an enzyme to insulin molar ratio of 1:50. Reactions were stopped by the addition of 30 μl of stop solution (170 mM EDTA, 0.07% trifluoroacetic acid). For MALDI/TOF analysis, 5 μl of reaction sample was mixed with 5 μl of 0.1% trifluoroacetic acid and purified using Zip-Tip C18 columns (Millipore). Sample was then mixed with 1 μl of matrix, α-cyano-4-hydroxycinnamic acid in 70% acetonitrile and 0.1% trifluoroacetic acid, and 0.7 μl of the mixture was spotted on the metal plate. Mass spectra were obtained either in linear or positive reflector mode using a Voyager 4700 MALDI/TOF mass spectrometer (Applied Biosystems). The mass spectrometry data were analyzed by Data Explorer (Applied Biosystems), FindPept (ExPASy proteomics server), and SearchXlinks (20).

For LC-FTICR-MS, the IDE-digested insulin samples (2–6 μl) were injected into a nano-HPLC system (Dionex Ultimate 3000, Sunnyvale, CA) onto which was installed a Zorbax C18 trapping column (300 μm inner diameter × 5 mm; Agilent Technologies, Santa Clara, CA) running an isocratic buffer of 95% 0.1% formic acid in water, 5% acetonitrile. The trapping column retained the peptides injected thus allowing them to be washed, and then the peptides were eluted onto an analytical column (75 μm inner diameter × 150 mm, 300 Å pore size; Agilent Zorbax C8) using a gradient in which a mobile phase of 85% 0.1% formic acid in water, 15% acetonitrile is changed to a mobile phase of 75% 0.1% formic acid in water, 25% acetonitrile in 7 min, then to 45% acetonitrile in 17 min, and then finally to 80% acetonitrile in 25 min. The peptides eluted from the nano column at a flow rate of 200 nl/min and were sprayed into a Thermo LTQ-FT tandem MS instrument running Xcalibur software (version 2.2) equipped with a nanospray source using a New Objectives (Woburn, MA) picotip nanospray needle with an 8-μm inner diameter tip. Spectra were acquired using positive ion nano ESI mode with the FTICR acquiring precursor spectra from 250 to 1800 m/z at a resolution of 50,000 at m/z 400.

For ECD-MS/MS, spectra were acquired in a data-dependent manner using the five most intense ions with charge states of +2 or higher from each FTICR MS scan to trigger the LTQ into performing ECD on each of the selected precursor ions. Spectra were recorded from the linear trap portion of the instrument. ECD was performed within the ICR cell, allowing the system to select precursor ions that contained a minimum of three or more charges. The ECD parameters were 4 eV and an initial dissociation time of 100 ms, which were subject to variation based on the actual charge state of the precursors (the higher the charge state the shorter the dissociation time required) and two microscans per experiment at a resolution of 50,000 at m/z 400.

Spectra of putative disulfide-bonded peptides were confirmed by a subsequent run to specifically accumulate ECD MS/MS on previously detected peptides thought to contain a disulfide bond and produce dedicated tandem MS chromatograms of only those precursor ions throughout a chromatographic run. A method was created using the LC conditions previously described to repetitively run a multiscan event experiment consisting of a single MS scan event using the FTICR at a resolution of 25,000 at m/z 400 and then up to three additional dedicated MS/MS ECD scan experiments on preselected peptide masses at resolution of 50,000 at m/z 400 across appropriate scan ranges.

Data obtained from these experiments were then extracted and qualitatively examined to confirm the masses and charge states of putative fragment ions arising from the direct cleavage of disulfide bonds. Accurate precursor ion masses were extracted from the MS portion of each experiment using either the program Xtract (Thermo Instruments, Waltham MA) or the program Hardklor to generate an accurate neutral mass for each peptide. Lists of the peptide masses were submitted to the program SearchXLinks (20) and searched against the putative sequence of insulin, allowing for specific intramolecular crosslinks between cysteines on the one or two chains of each protein. The results were used to guide the analysis of possible disulfide-bonded peptides using the ECD technique.

Enzymatic Competition Assay—Enzyme activities were assayed using a fluorogenic bradykinin-mimetic substrate of IDE, substrate V (7-methoxycoumarin-4-yl-acetyl-RPPGF-SAFK-2,4-dinitrophenyl, R & D Systems) (2, 14, 21). Competition reactions were carried out at 37 °C by mixing 90 μl of 0.5 μM substrate V in 50 mM potassium phosphate buffer, pH 7.3, and 10 μl of human insulin (Sigma) at the desired concentrations. The reactions were initiated by the addition of 5 μl of 0.2 mg/ml IDE protein. The substrate V degradation was assessed by monitoring fluorescence intensity for 10 min every 20 s on a Tecan Safire^2 microplate reader (λ_{ex} = 327 nm, λ_{em} = 395 nm).

Isothermal Titration Calorimetry—ITC data were collected for the binding of insulin to IDE and IDE-CF mutant. ITC titrations were carried out at 25 °C using a VP-ITC instrument (MicroCal, Northampton, MA). In a typical experiment, before the titration, insulin and IDE were dialyzed against 800 volumes of 20 mM Tris-HCl, pH 7.7, 50 mM NaCl at 4 °C overnight. Ligand, protein, and reference buffer solutions were degassed under vacuum prior to experimentation. The IDE solution (1.43 ml of 6 μM in dialysis buffer) in the ITC cell was titrated with insulin (30 μM in dialysis buffer) loaded into the ITC syringe. The first injection (2 μl, omitted from analysis) was followed by 30 injections of 10 μl with 200-s intervals between injections. Experiments were carried out in triplicate. MicroCal Origin software (version 5.0) was used to fit ITC curves using a two-site binding model.

Analytical Ultracentrifugation—Sedimentation equilibrium experiments were carried out using an Optima XL-A analytical ultracentrifuge (Beckman Coulter) with a 60-Ti rotor at 25 °C and 45,000 rpm, with standard Epon double-sector centerpieces equipped with quartz windows. The centerpieces were scanned from a minimum radius of 5.8 cm to a maximum radius of 7.3 cm. Sedimentation data were acquired at a wavelength of 230 nm and a radial spacing of 0.001 cm. The protein samples were diluted to 250–500 nM using 20 mM potassium phosphate, pH 7.3, and insulin was added in a 1:2 molar ratio when desired. Data were analyzed using SEDPHAT.

Insulin Iodination—Iodination of insulin was performed as described previously in the final molar ratio of insulin to iodide of 1:5 (22, 23). The iodinated insulin was purified by Superdex Peptide 10/300 GL column (GE Healthcare) and concentrated by ultrafiltration using Centricon® 3,000 molecular weight cutoff (Millipore). The presence of iodine in insulin was verified by mass spectrometry using the Voyager 4700 MALDI/TOF mass spectrometer.

Protein Crystallization—To crystallize catalytically inactive IDE-CF-E111Q in complex with insulin or iodinated insulin, IDE-CF-E111Q was incubated with insulin in a 1:1 molar ratio at 4 °C for 1 h before application to a Superdex 200 column (GE Healthcare) previously equilibrated with a $T_{20}N_{50}$ (20 mM Tris-HCl, pH 8.0, 50 mM NaCl) buffer. The peak fractions of IDE were concentrated by Centricon®. The steps of incubation and isolation of the IDE-insulin complex were repeated five times to ensure high purity and occupancy of the IDE-insulin complex. Prior to the last gel filtration step, the substrate to enzyme molar ratio was increased to 2 during the incubation step. Immediately following protein purification and concentration, 1 μl of protein (16–20 mg/ml) and 1 μl of crystallization solution (10–13% polyethylene glycol MME 5000, 100 mM HEPES, pH 7.0, 4–14% Tacsimate, 10% dioxane) were mixed and equilibrated with 500 μl of well solution at 18 °C by hanging drop vapor diffusion. Crystals appeared in 3–5 days and were sequentially equilibrated in 15 and 30% glycerol cryoprotective solutions containing reservoir buffer before being flash-frozen in liquid nitrogen.

Data Collection and Structure Determination—Diffraction data were collected at 100 K at the Advance Photon Source 14-BM-C and 19-ID beamlines at Argonne National Laboratory. The data set of insulin-bound IDE was collected at 13.8 keV, whereas that of iodinated insulin-bound IDE was collected at 8 keV for the maximal anomalous signal with the stable x-ray beam. The data sets were processed using HKL2000 (24). The crystals belong to space group $P6_5$ with unit cell dimensions $a = b = 263$ Å and $c = 90$ Å and contain a dimeric complex per asymmetric unit. Molecular replacement using Aβ-bound IDE-E111Q structure as a search model (PDB code 2G47) was performed with the program Phaser (25). Structure refinement and rebuilding were performed using REFMAC and Coot (26, 27). The extra electron density at the catalytic chamber of IDE in the iodinated insulin-bound and insulin-bound IDE was clearly visible based on σ_A-weighted $F_o - F_c$ map calculated by CNS (28). Insulin A and B chains in the structure of iodinated insulin-bound IDE-CF-E111Q were manually built by assessing the σ_A-weighted $2F_o - F_c$ and $F_o - F_c$ difference electron density maps. The anomalous difference map was used to identify and confirm the locations of tyrosine 14 and 19 of insulin A chain. For the structure of insulin-bound IDE, the σ_A-weighted $F_o - F_c$ difference map revealed that the insulin orientation in insulin-bound IDE was similar to that of iodinated insulin-bound IDE. Thus, an insulin molecule was placed in the catalytic chamber accordingly, and the structure of insulin-bound insulin was then refined. The composite omit maps were calculated to confirm the orientation of substrates. Figures were generated using PyMol (29) and CCP4MG (30). The volumes of the catalytic chamber of IDE and that of insulin were calculated using VOIDOO (31), and shape complementarity was calculated as described (32).

RESULTS

MALDI-TOF Analysis of the Degradation of Human Insulin by Human IDE—The determination of the precise cleavage sites and reaction products was originally derived from the HPLC profile of individually purified, reduced insulin fragments, and the termination of Edman degradation of porcine [^{125}I]iodo-insulin cleaved by rat IDE (4, 15, 16). However, these methods suffer from low sensitivity and low throughput. Recently, the cleavage products of bovine insulin by recombinant rat IDE were analyzed by atmospheric pressure/matrix-assisted laser desorption ionization (MALDI)/mass spectra (MS) analysis (17, 18). However, the chosen mass spectrometry method has relatively low mass accuracy and resolution. In addition, the reaction products of cleaved A and B chains linked by disulfide bond(s) are inferred from the mass derived from cleavage sites of the reduced samples and not directly derived from the fragmentation of precursor ions. Neither study performed the careful time-dependent production of IDE-degraded fragments to determine whether IDE cleaves insulin in a sequential or stochastic manner. Moreover, the reactions were performed using insulin and IDE from a different species. To our knowledge, the reaction products of human insulin cleaved by human IDE have not been reported. Thus, the precise reaction products of human insulin by human IDE, the time-dependent creation of these products, and the precise path(s) by which IDE unfolds insulin leading to the given cleavage products are unclear.

To study how human IDE degrades human insulin, we expressed and purified the recombinant human IDE from

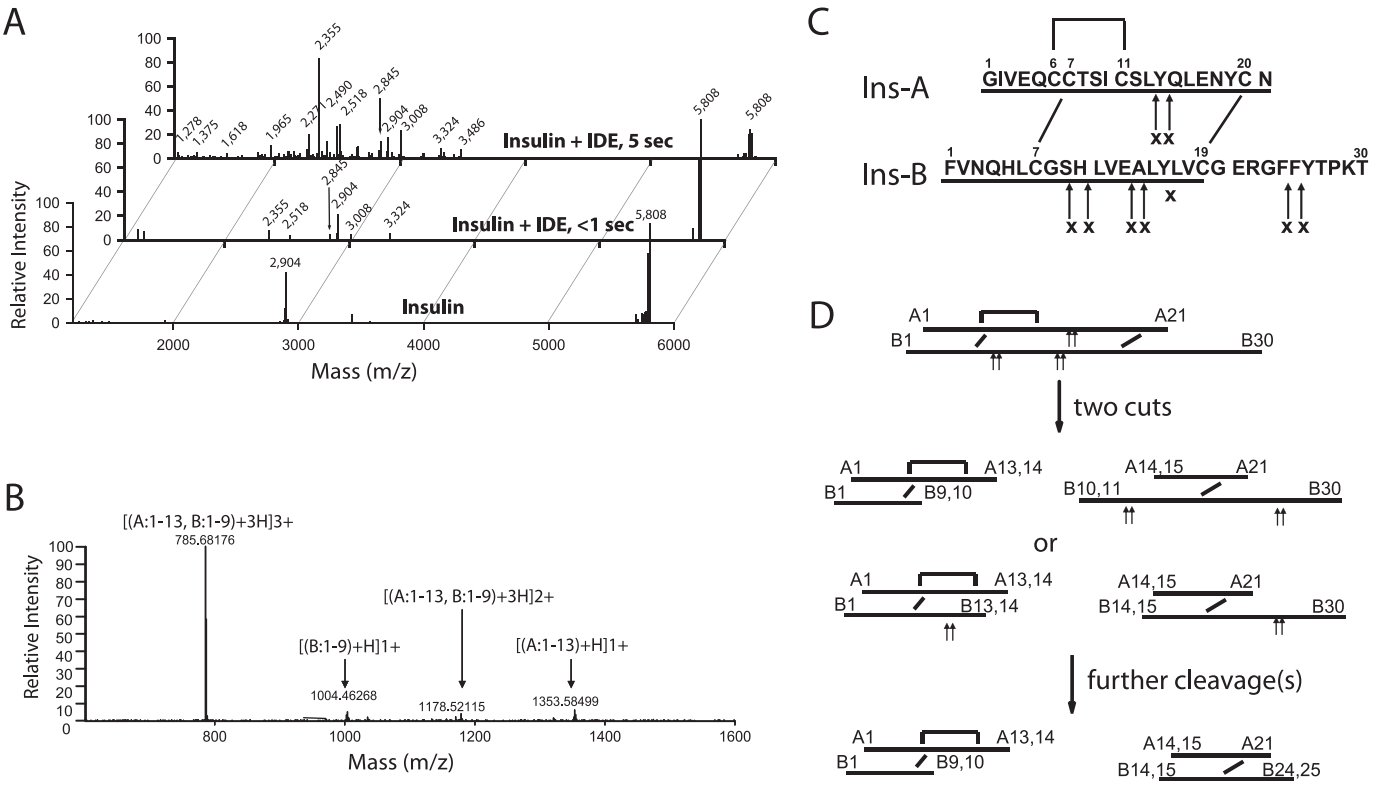

FIGURE 1. **Characterization of insulin degradation by IDE.** *A,* MALDI-TOF mass spectra of insulin (*bottom*) and IDE-degraded insulin (*upper two panels*). Insulin and IDE were mixed in a 50:1 molar ratio. After less than 1- and 5-s incubations, EDTA (170 mM) and trifluoroacetic acid (0.07%) were added to stop the reactions. *B,* representative ESI-EC mass of 2,354 Da. *C,* primary sequence and IDE cleavage sites of human insulin (*Ins*). Disulfide bonds are shown by a *line* connecting two cysteines. *Arrows* depict the cleavage sites of IDE by our FTICR-MS-ECD-MS/MS analysis, and *x* mark the sites found by previous studies (4, 15–17). *D,* model of the degradation of insulin by IDE.

E. coli and performed the digestion of human insulin by IDE. Human IDE can rapidly degrade human insulin into many pieces (Fig. 1*A*). We characterized the IDE-degraded fragments using MALDI-TOF-MS. Using 80 μM insulin, which is significantly higher than the K_m value (85 nM), and the time-dependent production of a major cleavage product, 2,355 Da, the estimated catalytic rate is $\sim$2 s^{-1}. This is in reasonable agreement with the known rate (0.5 s^{-1}) determined by using ^{125}I-labeled insulin (33).

After a less than 1-s incubation, five major IDE-degraded insulin fragments (2,355, 2,518, 2,845, 3,008, and 3,324 Da) were obtained (Fig. 1*A*). After a 5-s or longer incubation, $\sim$21 IDE-degraded insulin fragments could be identified (Fig. 1*A* and supplemental Table S1). This indicates that the cleavage of insulin by IDE is a nonrandom process and likely follows a defined path. We also found that IDE exhibits high processivity in the first two cleavages of insulin. No single-cut insulin fragment was observed even under conditions where greater than 95% intact insulin remains (Fig. 1*A*). The insulin A and B chains are held by two inter-chain disulfide bonds. If a cleavage occurs in the region outside these two disulfide bonds, single cleavage of insulin by IDE will result in fragments with sizes between 4,400 and 5,808 Da (the size of intact insulin). If a single cleavage of insulin occurs within the two intermolecular disulfide bonds, a single hydrolysis reaction should yield a 5,826-Da fragment. No such reaction products were observed (Fig. 1*A* and supplemental Table S1). Therefore, the cleavage of insulin by IDE is highly processive in its initial cuts.

Assignment of IDE-degraded Insulin Fragments Using FTICR-MS-ECD-MS/MS—Given the fact that the IDE-degraded insulin fragments were previously determined by inferring their composition from the reduced samples using atmospheric pressure/MALDI/MS, which also suffers from low mass accuracy and resolution (17, 18), we subsequently applied ECD as the gas phase fragmentation method and tandem mass spectrometry (MS/MS) to directly identify the composition of IDE-degraded insulin fragments. Two inter- and one intra-chain disulfide bonds in insulin pose a significant challenge for the identification of each fragment. Under conditions of collision-induced dissociation normally used in the tandem MS of peptides, the presence of disulfide bonds would produce complex spectra (data not shown). The complex spectra derived from high charge state ions formed from high mass peptides are particularly difficult to interpret and assign sequence unambiguously. To overcome this problem, we chose to use ECD for our MS/MS. ECD has been shown to be a very efficient method for producing interpretable product ion spectra from high charge state high mass ions such as those produced from proteins in the gas phase (34, 35). Furthermore, disulfide bonds in proteins are preferred sites for fragmentation under ECD conditions (36). This is presumably due to the intra-molecular hydrogen bonds from protonated side chains near the disulfide bonds (37). Because multiple charged states are required for acceptable ECD spectra, electrospray ionization (ESI) was chosen (36).

The presence of multiple disulfide bonds in insulin also allows many possible sequence combinations to be derived for

TABLE 1
Summary of mass spectrometry analysis of disulfide-bond linked IDE-degraded insulin fragments

Ins-A	Ins-B	A-B(observed) M + H	A-B(calculated) M + H	Error[a]	A (observed) *m/z*	A (calculated) *m/z*	Error[a]	B (observed) *m/z*	B (calculated) *m/z*	Error[a]
				ppm			*ppm*			*ppm*
N-terminal insulin fragments[b,c]										
1–13	1–9	2355.031	2355.024	3.0	1353.585	1353.585	−0.2	1004.463	1004.462	0.3
1–13	1–10	2492.095	2492.082	0.7	1353.588	1353.585	2.0	1141.495	1141.521	−22.7
1–14	1–9	2518.089	2518.087	0.8	1516.630	1516.648	−12.1	1004.463	1004.462	0.7
1–14	1–10	2655.178	2655.146	12.0	1516.640	1516.648	−5.4	1141.550	1141.521	25.1
C-terminal insulin fragments[d]										
14–21	14–30	3008.402	3008.396	2.0	1046.426	1046.425	0.9	982.996	983.001	−5.1
15–21	10–30	3323.578	3323.587	−2.4	883.389	883.362	30.3	1222.181	1222.128	43.6
C-terminal insulin peptides with an additional C-terminal cleavage at the insulin B chain[e]										
14–21	14–25	2418.092	2418.089	1.2	1046.432	1046.425	7.0	1374.684	1374.688	−3.0
14–21	14–24	2271.042	2271.021	9.2	1046.434	1046.425	8.6	1227.629	1227.620	7.6
14–21	15–25	2347.044	2347.052	−3.4	1046.417	1046.425	−8.1	1303.646	1303.651	−3.3
15–21	14–25	2255.019	2255.026	−3.1	883.361	883.362	−1.6	1374.684	1374.688	−3.0

[a] Error (in ppm) = $((M + H)_{obs} - (M + H)_{calc})/(M + H)_{calc} \cdot 10^6$.
[b] Assignment is shown of the most prominent insulin peaks generated after 5 min of incubation with IDE using LC-ESI-FTICR-MS-ECD-MS/MS.
[c] Four insulin fragments resulting from the cleavages at either A13–14 or A14–15 once and at either B9–10 or B10–11 once were observed. Insulin fragment containing A1–13 and B1–13 was observed, which is 1 of four possibilities from the cleavages at either B13–14 or B14–15 in conjunction with a cleavage in chain A (supplemental Table S1).
[d] Four insulin fragments resulting from the cleavages at either A13–14 or A14–15 once and at either B113-14 or B14–15 once were observed. Insulin fragment containing A15–21 and B10–30 was also observed, which is one of four possibilities from the cleavages at either B9–10 or B10–11 in conjunction with a cleavage in chain A (supplemental Table S1).
[e] Out of eight possible insulin fragments, all were observed by either FTICR-MS or MALDI-TOF-MS (supplemental Table S1).

any given observed peptide mass. For example, there are 11 possibilities that are within 4 ppm error tolerance for the 2,355-Da species identified by MALDI-TOF, a major product of IDE-degraded insulin (Fig. 1*A* and supplemental Fig. S1). Thus, ECD-MS/MS is vital to unambiguously assign the correct A/B chains within each insulin fragment. IDE-degraded insulin was passed through an HPLC C18 column to allow for some separation of cleavage products and therefore ensure maximal sampling of low abundance insulin fragments. FTICR mass spectrometry was used for its compatibility with ECD and the high mass accuracy and high resolution detection of both precursor and product ion spectra (38).

Using LC-ESI-FTICR-MS-ECD-MS/MS, we identified 10 IDE-degraded insulin fragments (Table 1, Fig. 1*B*, and supplemental Fig. S2). This is based on the excellent match of the observed mass from FTICR-MS of IDE-degraded insulin fragments with the predicted mass (Δppm $\leq$12) (Table 1). The identity of fragments from insulin A and B chains was revealed by ions from ECD-MS/MS (Fig. 1*B*, supplemental Fig. S2, and Table 1). For example, the insulin fragment with mass 2355.031 Da matches well with the predicted mass of an insulin fragment containing A1–A13 and B1–B9 peptides linked by one intra- and one inter-molecular disulfide bonds (Δppm = 3). The ion with the mass of 2,355 Da was analyzed simultaneously by data-dependent ECD-MS/MS in which selection and activation were favored for a precursor ion with at least three or more charges. ECD induces the breakage of the intermolecular disulfide bond to reveal ions that match well with A1–A13 and B1–B9 peptides (Δppm = −0.2 and 0.3, respectively). For some insulin fragments, we were only able to obtain FTICR-MS data, presumably due to their low abundance and/or the dependence of local environment around the targeted disulfide bond. However, the mass accuracy from FTICR allows the unambiguous assignment of these fragments (supplemental Table S1).

Model for the Path of Human Insulin Degradation by Human IDE—Based on our mass spectrometry study, the major cleavage sites of human insulin by recombinant human IDE are distributed to four discrete regions, each with two cleavage sites that are adjacent to each other (Fig. 1*C*). Three of these are located in the middle of either the A or B chain of insulin, and the last one is near the end of the B chain. No cleavage occurs near the N-terminal ends of either A or B chain. No clear sequence preference emerges from these sites. These sites matched well with those sites derived from the HPLC profile and the termination of Edman degradation of porcine [^{125}I]iodo-insulin cleaved by rat IDE (4, 15, 16) and MS analysis of bovine insulin cleaved by recombinant rat IDE (17). Different from previous findings, we did not observe the cleavage between B16 and B17 of human insulin by human IDE. It is worth noting that this site is the preferred binding and cleavage site of isolated insulin B chain by IDE (2).

The novel method of directly acquiring highly accurate masses both for the nonreduced insulin A-B chain fragment and for the individual A and B chain fragments of any given ion species allows the unambiguous assignment of the insulin fragments. Using such assignment, we then compared the cleavage products of insulin after a brief incubation with IDE (<1 s) with those from longer incubations (5 s (Fig. 1*A*) or longer (data not shown)). At the less than 1-s incubation, we observed five major products, 2,355, 2,518, 2,845, 3,008, and 3,324 Da, corresponding to insulin fragments of A1–13/B1–9, A1–14/B1–9, A15–21/B14–30, A14–21/B14–30, and A15–21/B10–30, respectively (Fig. 1*A*). All of these fragments can be created by two cleavages of insulin, one at chain A (either A13–14 or A14–15) and the other in the middle of chain B (B9–10, B10–11, B13–14, or B14–15). Under this incubation, no insulin fragment is derived from the cleavage at the C-terminal end of chain B (B24-B25 or B25–26; Fig. 1*A*, Table 1, and supplemental Fig. S1). The accumulation of insulin fragments containing the C-terminal cleavage of chain B occurred only after a longer time of incubation (5 s shown in Fig. 1*A* or longer (not shown)). This indicates that the cleavages at the C-terminal end of chain B (B24–25 and B25–26) occur later than those in the middle of insulin A and B chains. We also did not observe insulin frag-

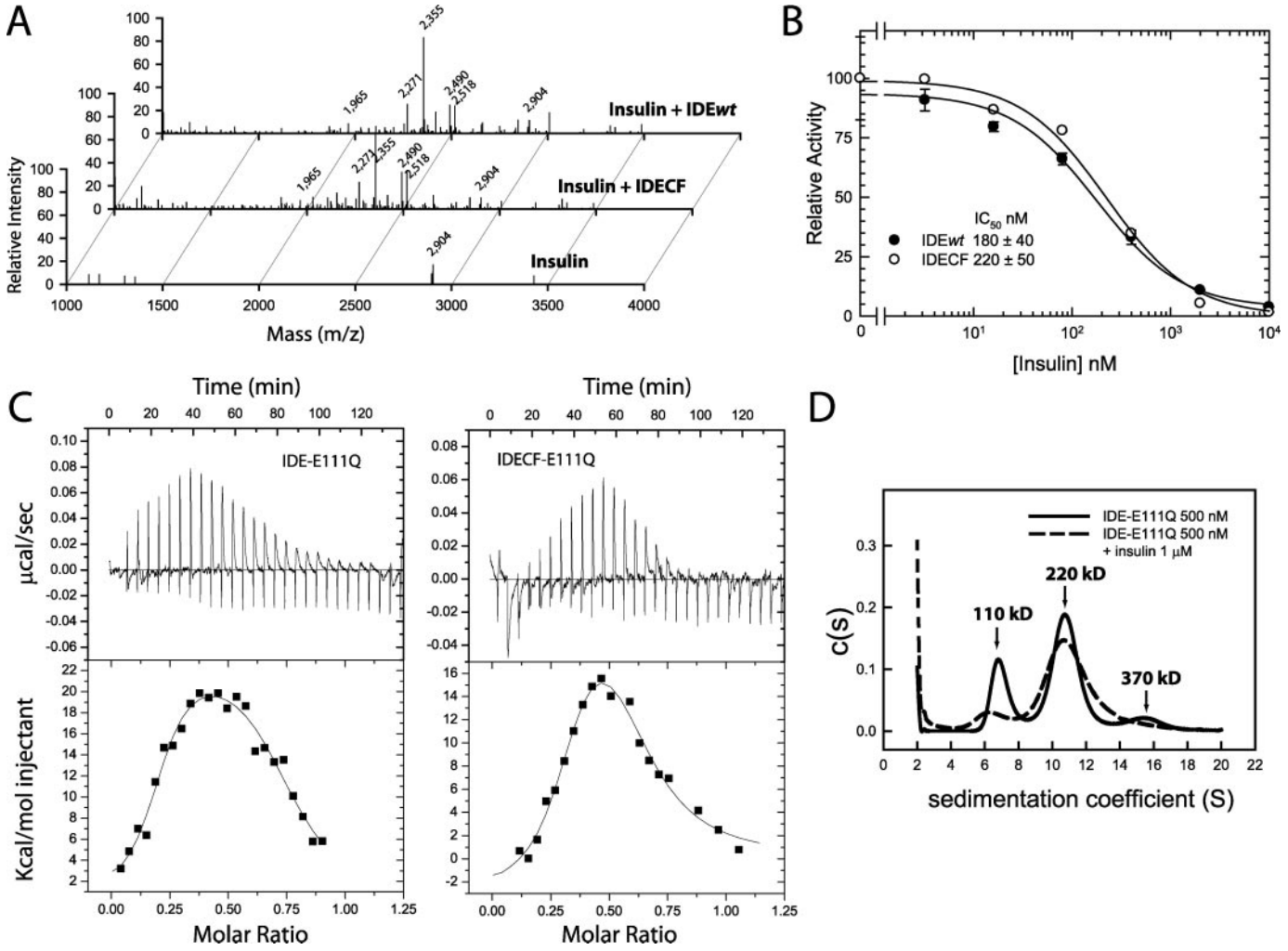

FIGURE 2. **Characterization of cysteine-free IDE.** *A,* MALDI-TOF mass spectra of insulin alone (*bottom*), insulin after 5 s of incubation with cysteine-free IDE (*IDECF, middle*) and wild type IDE (*IDEwt*, *top*). The peak with molecular mass of 2,904 Da represents the doubly charged state of undigested insulin. *B,* competition of substrate V degradation by IDE*wt* and IDE-CF by insulin. Substrate V (450 nM) was mixed with 1 μg of IDE*wt* or IDE-CF in the indicated concentrations of insulin (0–10 μM), and fluorescence intensity was monitored for 10 min at 37 °C. Results are means ± S.D. and are representative of three independent experiments performed in duplicate. *C,* isothermal calorimetry titration of insulin binding to IDE*wt*-E111Q and IDE-CF-E111Q with raw data (*top*) and the integrated heat signals (*bottom*). The *solid line* represents a calculated curve using the two-site binding model. Experiments were carried out in triplicate at 25 °C with IDE at 6 μM in 20 mM Tris-HCl, pH 7.7, 50 mM NaCl. The single spike corresponds to the heat exchange upon the addition of 10 μl of insulin (30 μM). Experiments were carried out in triplicate. *D,* sedimentation coefficient distributions for IDE-E111Q in the absence and presence (1:2 molar ratio) of insulin.

ments with multiple cuts at chain B without a cut in insulin A chain (supplemental Table S1).

From the time-dependent formation of insulin fragments by IDE, we constructed a model on how IDE sequentially cleaves insulin (Fig. 1*D*). IDE initiates the degradation of insulin by cleaving once at chain A and at least once in the middle of chain B. Such cleavages result in insulin fragments that contain either N-terminal or C-terminal portions of insulin (Fig. 1*D* and supplemental Table S1). The resulting insulin fragments are subsequently cleaved by IDE at the known cleavage sites of insulin B chain. This leads to the generation of insulin fragments with greater mass diversity as seen in the longer incubation with IDE.

Characterization of Cysteine-free IDE Mutant—The structure of insulin-bound IDE would provide insights into the molecular basis of the high affinity interaction between IDE and insulin and on the sequential cleavages of insulin. Unfortunately, the previously defined crystallization condition of human IDE requires the use of a reducing agent, tris(2-carboxyethyl)phosphine, presumably to protect IDE from oxidative inactivation (2). Under this condition, we only obtained the structure of IDE in complex with insulin B chain even though insulin was added, and the minimally required amount of reducing agent was used (2). To eliminate the need for a reducing agent, we constructed a human IDE mutant, IDE-CF, that is free of cysteine residues (supplemental Fig. S3) (19). The *in vitro* enzymatic assay showed that IDE-CF had catalytic activity comparable with wild type IDE in degrading insulin (Fig. 2*A* and supplemental Fig. S4). In addition, the ability of insulin to compete with the cleavage of a model substrate by IDE-CF is comparable with that of wild type IDE (Fig. 2*B*).

We also used ITC to evaluate the binding affinity of IDE to insulin (Fig. 2*C*). To avoid the degradation of insulin by IDE, a glutamate 111 to glutamine mutation was introduced into the catalytic site. Our ITC data fit well with a two-binding sites

TABLE 2
Data collection and structure refinement statistics of substrate-bound IDE

	IDE-insulin	IDE-iodinated insulin
Data collection		
Beamline	APS 14-BMC	APS 19ID
Wavelength	0.90020 Å	1.54980 Å
Space group	$P6_5$	$P6_5$
Cell dimension		
a	262.3 Å	263.2 Å
b	262.3 Å	263.2 Å
c	90.6 Å	90.8 Å
Resolution	50-2.6 Å	50-2.8 Å
R_{sym}[a] (%)	12.6 (49.6)[b]	11.0 (46.5)
I/σ	21.7 (4.8)[b]	18.2 (3.6)
Redundancy[c]	7.0 (6.5)[b]	5.4 (4.6)
Completeness (%)	99.9 (100.0)[b]	99.6 (98.3)
Figure of merit	0.871	0.873
Unique reflections	109,017	98,447
Refinement		
R_{work}[d]	0.164	0.170
R_{free}[e]	0.218	0.221
No. of atoms		
Protein	16,204	16,235
Water	721	360
B-factors		
IDE	27.5	36.4
Substrate	49.2	52.4
Water	31.7	36.4
Root mean square deviations		
Bond lengths	0.015 Å	0.016 Å
Bond angles	1.851°	1.941°
Ramachandran plot		
Favorable	91.0/88.7%	89.0/88.6%
Allowed	9.0/11.3%	11.0/11.4%
Generously allowed	0/0%	0/0%
Disallowed	0/0%	0/0%
PDB code	2WBY	2WC0

[a] $R_{merge} = \Sigma(I - \langle I\rangle)/\Sigma\langle I\rangle$.
[b] The outer resolution shell is shown. Values in parentheses indicate the highest resolution shell.
[c] N_{obs}/N_{unique}.
[d] $R_{work} = \Sigma_{hkl}||F_{obs}| - k|F_{calc}||/\Sigma_{hkl}|F_{obs}|$.
[e] R_{free}, calculated the same as for R_{work} but on the 5% data excluded from the refinement calculation.

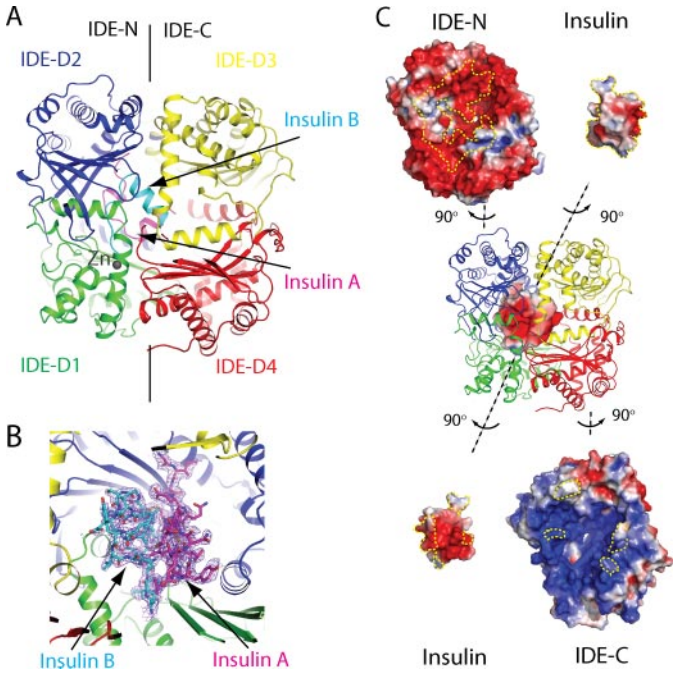

FIGURE 3. **Structure of insulin-bound IDE.** *A,* global view of the structure of insulin-bound IDE-CF-E111Q monomer. IDE domains 1–4 (*IDE-D1* to *IDE-D4*) are colored *green*, *blue*, *yellow*, and *red*, respectively. Insulin A and B chains are colored *magenta* and *cyan*, respectively. The zinc ion is colored *gray*. *B,* composite omit map of insulin contoured at 1.5σ. *C,* electrostatic surface representation of insulin and IDE. The molecular surface is color-coded as calculated by Adaptive Poisson-Boltzmann Solver. The molecular surface is colored as calculated by Adaptive Poisson-Boltzmann Solver (51) (<-6 *kT* in *red*, 0 kT in *white*, and $>+6$ kT in *blue*). The interaction surface between the N- and C-terminal domains of IDE and insulin is marked by *yellow dashed lines* based on the contact residues displayed using CCP4 molecular graphics (30).

model, and the estimated dissociation constant of the two sites are 10 and 140 nM. Although the functional unit of IDE is a monomer, hydrodynamic analyses reveal that, dependent upon the experimental conditions, IDE can shift to a dimer and even higher oligomers (21). Using analytical ultracentrifugation, we found that insulin can shift the equilibrium of monomeric IDE to be mostly a dimer (Fig. 2*D*). The presence of two insulin-binding sites of IDE might reflect the dimeric state of the enzyme. Similar to wild type IDE-E111Q, our ITC data showed that IDE-CF-E111Q also has two insulin-binding sites with comparable K_d values (20 and 280 nM). Together, our data indicate that the cysteine mutations do not alter the binding affinity of IDE for insulin or the ability of IDE to cleave insulin. Thus, IDE-CF represents an excellent model to investigate insulin binding.

Structure of IDE-Insulin Complex—We subsequently solved crystal structures of the catalytically inactive IDE-CF-E111Q in complex with human insulin and iodinated insulin at 2.6 and 2.8 Å resolution, respectively (Table 2, supplemental Fig. S5, and supplemental Fig. S6). Anomalous signals from iodine atoms of the iodinated insulin were used as a guide in the model building of insulin (supplemental Fig. S5). Here we focus on the insulin-bound IDE structure because iodinated insulin sits in the catalytic chamber of IDE in a virtually identical fashion as insulin. In accordance with our previously determined IDE-E111Q structures, IDE-CF is a dimer, and the four structurally homologous domains of each monomer form a large, enclosed catalytic chamber with a total volume of $\sim 1.6 \times 10^4$ Å^3 (Fig. 3 and supplemental Fig. S7), which is slightly larger than that of the T-state of an insulin monomer ($\sim 1.2 \times 10^4$ Å^3) (2, 39). An insulin molecule is completely encapsulated by each IDE monomer (Fig. 3*A*). Electron density maps for the majority of insulin A chain (A1–A20, 20 of 21 residues) and over three-fifths of insulin B chain (B1-B19, 19 of 30 residues) are clearly visible inside the catalytic chamber of IDE, where the peptide occupies ~64% of the space (Fig. 3*B*). The remaining portion of insulin (A21 and B20–B30) is not visible in the electron density maps, presumably due to disorder because intact, nondegraded insulin was found in insulin-bound IDE crystals by mass spectrometry (supplemental Fig. S6).

Our insulin-bound IDE structure reveals that the charge complementarity contributes significantly to the interaction of insulin with the catalytic chamber of IDE. IDE-N and IDE-C serve as the functional units to form the catalytic chamber (Fig. 3*C*) (21). The inner catalytic chamber of IDE-C is highly positively charged, which complements well with the negatively charged surface of human insulin, an acidic protein with an isoelectric point of 5.3 (Fig. 3*C*). The N-terminal regions of insulin A and B chains make intimate interactions with the inner chamber of IDE-N (Fig. 3*C* and supplemental Fig. S7).

Molecular Details of the Interaction of Insulin with the Catalytic Chamber of IDE—Insulin makes extensive contacts with the catalytic chamber of IDE (buried surface of 1,758 Å^2) with excellent surface complementarity (surface complementarity score = 0.67) (supplemental Fig. S7) (32). The interaction of insulin with IDE-N accounts for the predominant buried surface (1,355 Å^2; surface complementarity score = 0.71). The N-terminal end of insulin A chain forms a β-sheet with IDE strand β12 within an evolutionarily conserved exosite of IDE at domain 2, which is crucial for binding of IDE substrates (Fig. 4*A*) (2, 14). In addition, the N-terminal end of insulin B chain binds to the catalytic cavity at domain 1 of IDE (Fig. 4*A*). There is a network of hydrogen bonds, salt bridges, and van der Waals interactions of insulin with both IDE-N and IDE-C (Fig. 4*A*) (2, 14).

The N-terminal end (B1–B8) of IDE-bound insulin B chain adopts an extended conformation, a hallmark of insulin T-state that is the physiologically active form of this hormone (39, 40). The overall structure of IDE-bound insulin is similar to that of the crystal structure of T-state insulin (Fig. 4*B*) (39). Because of its interaction with the catalytic chamber of IDE, the monomeric, IDE-bound insulin is partially unfolded judging by the loss of an α-helix, the gain of a disordered loop, and the increased exposure of hydrophobic residues (Fig. 4*B*). Insulin structures have been determined both by x-ray crystallography and NMR, and our IDE-bound insulin structure deviates significantly from structures of wild type insulin and insulin analogs at three discrete regions (41). By binding to the exosite of IDE, the N-terminal end of insulin A chain is converted from an α-helix to a β-strand. In addition, the C-terminal segment of insulin B chain (B20–B30) is disordered, which differs from the tight interaction of this segment with the central α-helix of insulin B chain in crystal structures of T-state insulin (39).

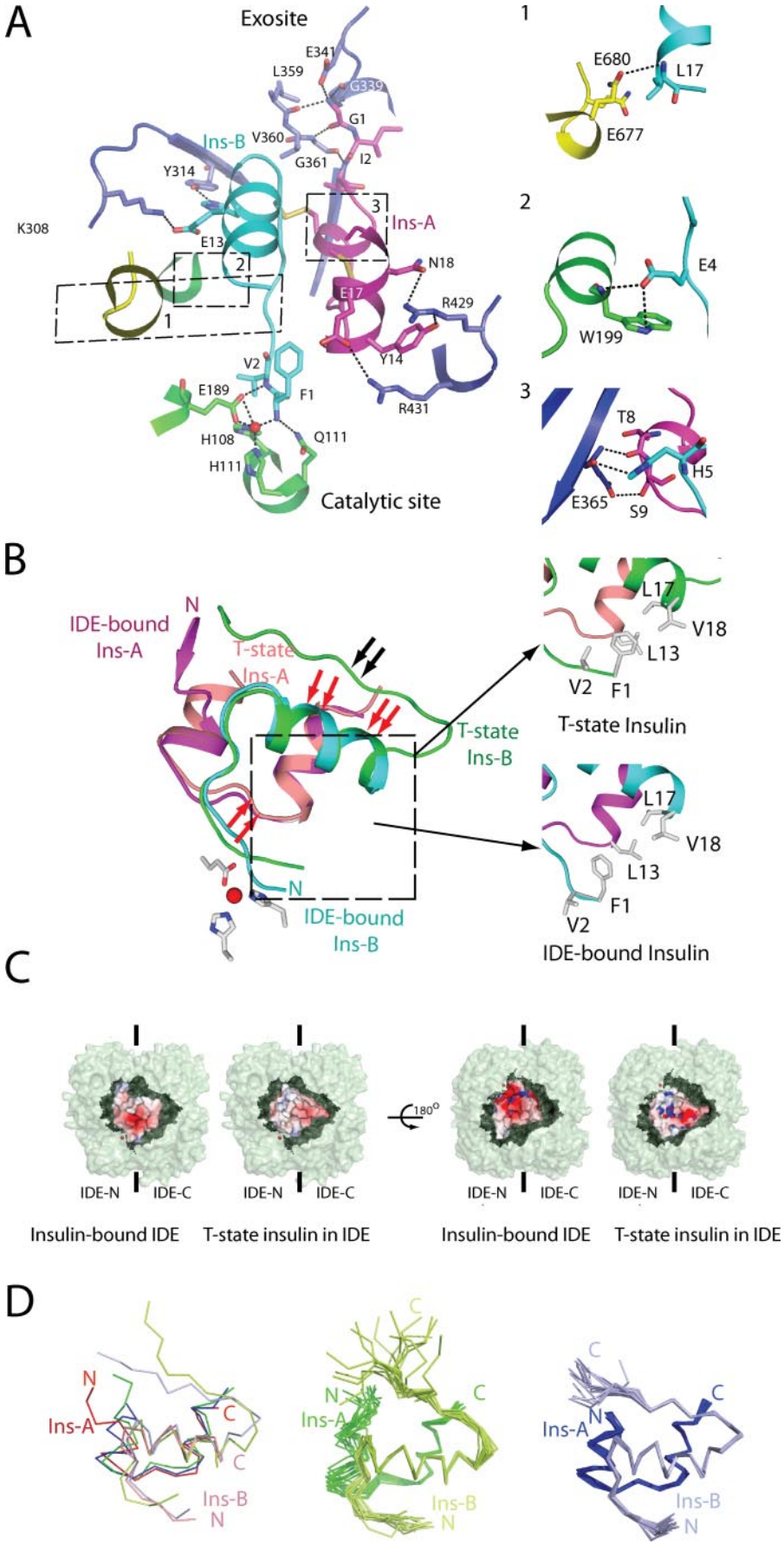

Furthermore, the interaction of Phe^1 at the N-terminal of the insulin B chain (Phe^1B) with the catalytic cavity of IDE pulls Phe^1B away from its interaction with the hydrophobic patch formed by $Leu^{17}B$ and $Val^{18}B$ (Fig. 4*B*). The surface charge distribution of the partially unfolded insulin inside the IDE catalytic chamber also differs significantly from that of T-state insulin (Fig. 4*C*). Most noticeably, the surface facing the catalytic chamber changes from a weakly positive to predominantly negative.

Our insulin-bound IDE structure likely represents how insulin binds to the catalytic chamber of IDE prior to its complete unfolding. The N-terminal end of the insulin B chain binds to the catalytic cavity at domain 1 of IDE with the peptide bond between Phe^1B and Val^2B near the catalytic zinc ion, resulting in an unfavorable interaction for water-mediated attack (Fig. 4, *A* and *B*). This is consistent with our observation that no cleavage is observed at the N-terminal end of insulin chain B (Fig. 1*A*). This also agrees with the distance between the catalytic ion and the observed cleavage sites of insulin. As described above, human IDE cleaves four discrete regions of human insulin, each containing two sites. These include one in the middle of A chain, two in the middle of B chain, and the other at the end of B chain. One cleavage in the A chain and another in the middle of B chain are required for the initial cleavages of insulin. Consistent with this, sites at the A chain are closest to the catalytic site (13 and 15 Å, respectively), and those sites in the middle of B chain are only slightly farther away (22, 20, 20, and 18 Å for B9–10, B10–11, B13–14, and B14–15, respectively). Although the cleavage sites at the end of B chain (B24–25 and B25–26) in our structure are disordered, their position would be farthest from the catalytic site of IDE. This is consistent with our mass spectrometry data suggesting that the cleavages at the end of B chain occur only after the initial cleavages in the middle of insulin A and B chains.

DISCUSSION

The degradation of human insulin by human IDE results in a complex mixture of disulfide bond-linked insulin fragments. The advance of proteomics-based mass spectrometry allows systemic study of the time-dependent production of the mixture of human insulin fragments cleaved by human IDE. In addition to using FTICR for its highly accurate mass determination of nonreduced insulin fragments, we also employed ECD as the gas phase fragmentation method to accurately identify fragments of insulin A and B chains from 10 precursor ions of the given insulin fragments. ECD-MS/MS spectra proved vital for our study because the commonly used peptide ID method, collision-induced dissociation-MS/MS, created extremely complex spectra due to the presence of disulfide bond(s) and suffered from the ineffective production of b and y ions around the disulfide bond(s) requisite for unambiguous peptide identification. Although ECD is postulated to be an effective method in the analysis of the labile post-translational modifications of proteins such as disulfide bonds (36), to our knowledge this is the first time that ECD-MS/MS is successfully used to decipher the composites of complex mixtures of biological samples. Further analysis of the composition of product ions and the molecular basis of disulfide bond breakage of insulin fragments from the ECD-MS/MS spectra will undoubtedly provide new insights into the chemical principles and future usage of ECD in proteomics analyses in biology and medicine.

Our mass spectrometry analysis reveals that IDE cuts in the middle of both the insulin A and B chains before cleaving the C-terminal end of the insulin B chain. Furthermore, IDE is highly processive to digest the middle of both the insulin A and B chains to produce N- and C-terminal halves of insulin fragments. Insulin has both inter and intra-chain disulfide bonds, so single cleavage of insulin by IDE will still allow the A and B chains to be held together for its binding and activation of insulin receptor. However, because both N- and C-terminal portions of the residues in the insulin A and B chains are involved in binding to the insulin receptor, either N- or C-terminal insulin fragment would be active in receptor binding and signal transduction (42–46). Thus, the processive cleavages of insulin by IDE ensure the complete inactivation of insulin without the need for subsequent binding and cleavage of the resulting insulin fragments (Fig. 1*D*).

Our insulin-bound IDE structure represents the first structure of insulin in complex with its biologically relevant protein partners. Three major conformational switches found in the IDE-bound insulin structure suggest insulin is in an intermediate unfolded state (Fig. 4, *B* and *D*). The disruption of an α-helix at the N terminus of the insulin A chain, the exposure of hydrophobic residues near the N terminus of the insulin B chain, and the disordered C-terminal loop of the insulin B chain are indicators of this partially unfolded conformation as all three changes are hallmarks of protein unfolding. Accumulating evidence indicates that protein folding follows certain routes, and the folding intermediates have substantial structural heterogeneity (47). Substrate unfolding inside the catalytic chamber of IDE likely follows the same principles. The lack of electron density outside the active site and exosite observed for other IDE-substrate complexes is consistent with the substantial disorder or heterogeneity of IDE substrates inside the catalytic chamber of IDE (2).

The binding of the N terminus of the insulin A chain to the exosite likely plays a key role in the catalytic chamber-assisted

FIGURE 4. **Characterization of the IDE-insulin interaction.** *A,* details of the interaction between insulin and IDE. Additional hydrogen bond networks are shown in the *three right panels* for clarity. IDE and insulin are colored as in Fig. 3. *B,* comparison of insulin in its free T-state form (PDB code 1G7A) and IDE-bound form. *C,* comparison of surface charge distribution of the partially unfolded insulin in insulin-bound IDE with T-state insulin modeled into the catalytic chamber of IDE. Surface representation of the substrate binding chamber of IDE was generated by the software Voidoo (31). The outer surface of IDE and the substrate chamber are colored *pale green* and *dark green*. The electrostatic surface representations of the IDE-bound insulin and T-state insulin models are calculated by Adaptive Poisson-Boltzmann Solver. *D,* comparison of IDE-bound insulin structure with the solution structures of insulin Ala^{A2}-DKP. Insulin Ala^{A2}-DKP has an Ile to Ala mutation in A2 residue of insulin-DKP, which is an engineered monomeric insulin. *Left* shows the comparison of IDE-bound insulin (colored in *red* and *salmon* for insulin A and B chain, respectively) with an exemplary NMR structure of insulin Ala^{A2}-DKP (PDB code 1K3M; colored in *green* and *lime green* for insulin A and B chain, respectively), and an exemplary NMR structure of insulin-DKP (PDB code 2JMN; colored in *blue* and *light blue* for insulin A and B chain, respectively). For a fair comparison, solution structures of insulin Ala^{A2}-DKP and insulin-DKP are also shown in the *middle* and *right*, respectively.

unfolding of insulin. When compared with >100 x-ray crystallographic and NMR structures of wild type insulin and insulin analogs, IDE-bound insulin is significantly different in the N-terminal end of the A chain as well as C-terminal tail of the B chain (Fig. 4, *B* and *D*). Interestingly, the IDE-bound insulin structure has an interesting resemblance of the NMR structures of insulin that bear an isoleucine to alanine mutation at residue 2 of the insulin A chain (Fig. 4*D*) (48). This single amino acid substitution is known to cause the decreased thermodynamic stability of insulin, which leads to disorder in the N-terminal A chain segment and more divergent C-terminal B chain tail. Thus, it is likely that the anchoring of the N-terminal A chain to the exosite of IDE that significantly alters the structure of the N-terminal end of insulin A chain as well also has a similar effect in reducing the thermodynamic stability of insulin to facilitate its unfolding.

Our insulin-bound IDE structure also reveals that the shape, size, charge distributions, conformational flexibility, and exosite binding of insulin all contribute to its tight binding (~100 nM) to IDE. During the proteolytic cycle, both IDE and its substrates undergo conformational switches (Fig. 5). IDE has open and closed conformational states (IDE^o and IDE^c), and the IDE substrates need to interact favorably with both states. The IDE^c state is stabilized by extensive contacts between IDE-N and IDE-C (1, 2, 14), making the IDE chamber inaccessible to substrates. Only in the IDE^o state can initial binding with the substrate occur. The dipolar charge distribution of insulin permits good charge complementarity with the catalytic chamber of IDE in the IDE^o state, with either the positively or negatively charged internal surfaces of IDE-C or IDE-N, respectively. The repositioning of IDE-N and IDE-C by the conformational switch of IDE^o to IDE^c allows insulin to interact simultaneously with the IDE-N and IDE-C surfaces of the catalytic chamber. The size and shape of insulin are also compatible with the fit into the chamber of IDE. As revealed by our insulin-bound IDE structure, the anchoring of the N-terminal end of the insulin A chain to the exosite of IDE occurs despite the lack of interaction of the targeted cleavage sites of insulin with the catalytic groove. This highlights the importance of the exosite interaction in determining the binding affinity of substrates (19).

In conjunction with our insulin-bound IDE structure, our data also allow us to construct a working model of how IDE processively cuts insulin into pieces (Fig. 5). Using MALDI-TOF-MS/MS and LC-FTICR-MS-ECD-MS/MS, we found that the initial cleavages of insulin by IDE occur in at least two locations, one in the middle of A chain and the other in the middle of B chain (Fig. 1*D*), resulting in the biologically inactive N- and C-terminal insulin fragments. Because IDE only has one catalytic center and the two selective cleavages are located at separate chains of insulin, IDE must have a mechanism to restrain the exit of singly cut insulin from the catalytic chamber so that the second cleavage can proceed immediately.

In our model, we postulate that the first cleavage of insulin occurs at one of two sites at the insulin A chain (Fig. 1*D* and Fig. 4*B*). This is based on the fact that these sites are closest to the catalytic site among all known cleavage sites. Furthermore, they are located in the middle of a loop that generally has a less stable structure than an α-helix, where the four cleavage sites of insulin B chain are located. The further unfolding of insulin from the partially unfolded insulin intermediate shown in our insulin-bound IDE structure allows one of the two adjacent cleavage sites on insulin A chain to swing into the catalytic site of IDE for cleavage (Fig. 5*B*). The N terminus of the insulin A chain is anchored to the highly conserved exosite of IDE (1, 2, 14). The exosite and other regions of the IDE catalytic chamber that contact insulin work as a reverse chaperone to guide insulin along the defined unfolding route(s). The structural heterogeneity present during the unfolding of insulin likely explains why it is a probabilistic process for IDE to cut either site in the insulin A chain. A cleavage at the insulin A chain does not separate insulin into two pieces. IDE substrates are known to interact with both IDE-N and IDE-C, which can serve to hold these two domains together (2, 14). Thus, the interaction of

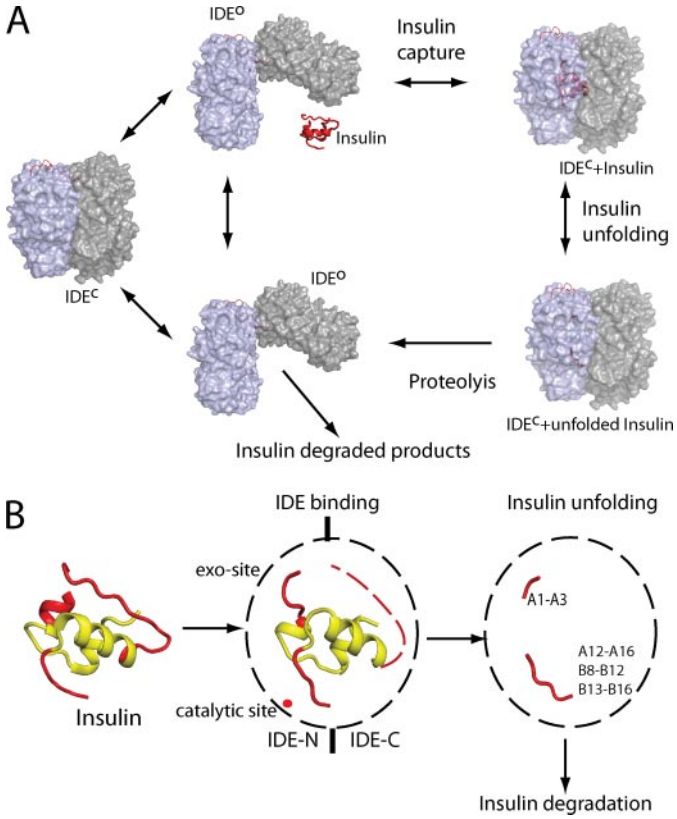

FIGURE 5. **Model of insulin degradation by IDE.** *A,* model for the conformational switch of IDE in the catalytic cycle of insulin degradation. Insulin is captured by IDE, and the structure of IDE^C + insulin depicts the state of the binding. Once insulin is captured by IDE^o, the conformational switch of IDE entraps insulin inside the catalytic chamber. This leads to the partially unfolded insulin depicted as IDE^c + insulin. For insulin digestion, insulin needs to undergo conformational changes. In this closed state, IDE likely performs at least two cycles of the unfolding and a single cleavage to generate the N- and C-terminal fragments depicted in Fig. 1*D* before releasing the cleavage products by switching back to an open state. IDE^o either goes back to the substrate-free IDE^c or captures another substrate (insulin or the resulting insulin fragments) for the next cycle. The substrate-free closed and the open state (IDE^c and IDE^o, respectively) are modeled based on substrate-free IDE^C (PDB code 2JG4) and *E. coli* pitrilysin structure (PDB code 1Q2L). The free-state insulin and IDE-bound insulin are depicted as *red* schematics. IDE-N and IDE-C are depicted as transparent *blue* and *gray* surfaces, respectively. The loop hinge of IDE is depicted as *red ribbon*. *B,* three possible states of insulin are shown, T-state (*left*), IDE-bound partially unfolded state (*middle*), and IDE-bound fully unfolded state (*right*). For comparison, the regions that undergo the major conformational changes are colored in *red,* and those that do not are colored *yellow*.

insulin with the internal chamber still allows insulin to hold IDE-N and IDE-C together to maintain the IDE^c state. The high stability of the IDE^c state also contributes to prolong the entrapment of insulin inside the catalytic chamber (14).

The next cleavage occurs at one of four sites located on the central helix of the insulin B chain (Fig. 4*B*). Not only are these sites farther away from the reaction center than those on the insulin A chain, but their access to the catalytic site is sterically hindered by the presence of the loop containing the cleavage sites of the insulin A chain. Thus, a cleavage in the insulin A chain would allow these sites on the insulin B chain to gain access to the catalytic site of IDE. Such cleavage could also trigger a conformational switch of the central α-helix of the insulin B chain to a loop, facilitating access to the catalytic groove of IDE (Fig. 5*B*). Again, the structural heterogeneity of the unfolding path allows any of the four sites to interact with and be cut by the catalytic site of IDE in a stochastic manner. Such cleavage will create N- and C-terminal fragments of insulin that are no longer covalently joined so that they cannot interact with IDE-N and IDE-C simultaneously and tie these domains together. This permits the formation of IDE^o, allowing the dissociation of insulin fragments. The released insulin fragments can subsequently bind IDE^o and are subject to further cleavages at other sites in the insulin B chain, particularly at its C-terminal end. The validity of this model awaits future biophysical and biochemical studies.

In summary, our analyses describe the molecular basis by which IDE recognizes, unfolds, and processively degrades insulin. They also highlight the role of the size and charge of the IDE catalytic chamber as well as the conformational flexibility of substrates as determinants of the substrate specificity of this protease. In addition, they reveal how the highly conserved exosite of IDE could anchor the N termini of IDE substrates, guiding the unfolding and cleavage of substrates in the catalytic chamber. Our model of how IDE processively degrades insulin also provides the framework for designing IDE-insensitive insulin. Such modified insulin would have a prolonged half-life in circulation, which could be further developed for better management of diabetes (5). Furthermore, the comparison of the insulin-bound IDE structure with Aβ-bound IDE offers an insight into the engineering of IDE that preferentially degrades Aβ. Such engineered IDE might serve as a protein-based therapeutic for the clearance of Aβ in the treatment of Alzheimer disease (49, 50).

Acknowledgments—We are grateful to the staff of Structural Biology Center and BioCars at Advanced Photon Source, Argonne National Laboratory, and Elena Solomaha at the Biophysics Facility, University of Chicago, for help in data collection. We thank Todd Funke, Yao Bian, and Ray Hulse for the helpful discussions and critical reviews. Use of the Advanced Photon Source was supported by the United States Department of Energy, Office of Basic Energy Sciences, under Contract W-31-109-ENG-38. Use of proteomics service facility was supported by the Chicago Biomedical Consortium.

REFERENCES

1. Malito, E., Hulse, R. E., and Tang, W. J. (2008) *Cell. Mol. Life Sci.* **65,** 2574–2585
2. Shen, Y., Joachimiak, A., Rosner, M. R., and Tang, W. J. (2006) *Nature* **443,** 870–874
3. Mirsky, I. A., and Broh-Kahn, R. H. (1949) *Arch. Biochem.* **20,** 1–9
4. Duckworth, W. C., Bennett, R. G., and Hamel, F. G. (1998) *Endocr. Rev.* **19,** 608–624
5. Farris, W., Mansourian, S., Chang, Y., Lindsley, L., Eckman, E. A., Frosch, M. P., Eckman, C. B., Tanzi, R. E., Selkoe, D., and Guenette, S. (2003) *Proc. Natl. Acad. Sci. U. S. A.* **100,** 4162–4167
6. Sladek, R., Rocheleau, G., Rung, J., Dina, C., Shen, L., Serre, D., Boutin, P., Vincent, D., Belisle, A., Hadjadj, S., Balkau, B., Heude, B., Charpentier, G., Hudson, T. J., Montpetit, A., Pshezhetsky, A. V., Prentki, M., Posner, B. I., Balding, D. J., Meyre, D., Polychronakos, C., and Froguel, P. (2007) *Nature* **445,** 881–885
7. Kurochkin, I. V., and Goto, S. (1994) *FEBS Lett.* **345,** 33–37
8. Kurochkin, I. V. (2001) *Trends Biochem. Sci.* **26,** 421–425
9. Kim, M., Hersh, L. B., Leissring, M. A., Ingelsson, M., Matsui, T., Farris, W., Lu, A., Hyman, B. T., Selkoe, D. J., Bertram, L., and Tanzi, R. E. (2007) *J. Biol. Chem.* **282,** 7825–7832
10. Leissring, M. A., Farris, W., Chang, A. Y., Walsh, D. M., Wu, X., Sun, X., Frosch, M. P., and Selkoe, D. J. (2003) *Neuron* **40,** 1087–1093
11. Miller, B. C., Eckman, E. A., Sambamurti, K., Dobbs, N., Chow, K. M., Eckman, C. B., Hersh, L. B., and Thiele, D. L. (2003) *Proc. Natl. Acad. Sci. U. S. A.* **100,** 6221–6226
12. Tanzi, R. E., and Bertram, L. (2005) *Cell* **120,** 545–555
13. Baker, T. A., and Sauer, R. T. (2006) *Trends Biochem. Sci.* **31,** 647–653
14. Im, H., Manolopoulou, M., Malito, E., Shen, Y., Zhao, J., Neant-Fery, M., Sun, C. Y., Meredith, S. C., Sisodia, S. S., Leissring, M. A., and Tang, W. J. (2007) *J. Biol. Chem.* **282,** 25453–25463
15. Davies, J. G., Muir, A. V., Rose, K., and Offord, R. E. (1988) *Biochem. J.* **249,** 209–214
16. Duckworth, W. C., Hamel, F. G., Peavy, D. E., Liepnieks, J. J., Ryan, M. P., Hermodson, M. A., and Frank, B. H. (1988) *J. Biol. Chem.* **263,** 1826–1833
17. Grasso, G., Rizzarelli, E., and Spoto, G. (2007) *J. Mass Spectrom.* **42,** 1590–1598
18. Grasso, G., Rizzarelli, E., and Spoto, G. (2008) *Biochim. Biophys. Acta* **1784,** 1122–1126
19. Malito, E., Ralat, L. A., Manolopoulou, M., Tsay, J. L., Wadlington, N. L., and Tang, W. J. (2008) *Biochemistry* **47,** 12822–12834
20. Wefing, S., Schnaible, V., and Hoffmann, D. (2006) *Anal. Chem.* **78,** 1235–1241
21. Li, P., Kuo, W. L., Yousef, M., Rosner, M. R., and Tang, W. (2006) *Biochem. Biophys. Res. Commun.* **343,** 1032–1037
22. Frank, B. H., Beckage, M. J., and Willey, K. A. (1983) *J. Chromatogr.* **266,** 239–248
23. Hamlin, J. L., and Arquilla, E. R. (1974) *J. Biol. Chem.* **249,** 21–32
24. Otwinowski, Z., and Minor, W. (1997) *Methods Enzymol.* **276,** 307–326
25. McCoy, A. J., Grosse-Kunstleve, R. W., Storoni, L. C., and Read, R. J. (2005) *Acta Crystallogr. Sect. D Biol. Crystallogr.* **61,** 458–464
26. Murshudov, G. N., Vagin, A. A., and Dodson, E. J. (1997) *Acta Crystallogr. Sect. D Biol. Crystallogr.* **53,** 240–255
27. Emsley, P., and Cowtan, K. (2004) *Acta Crystallogr. Sect. D Biol. Crystallogr.* **60,** 2126–2132
28. Brunger, A. T., Adams, P. D., Clore, G. M., DeLano, W. L., Gros, P., Grosse-Kunstleve, R. W., Jiang, J. S., Kuszewski, J., Nilges, M., Pannu, N. S., Read, R. J., Rice, L. M., Simonson, T., and Warren, G. L. (1998) *Acta Crystallogr. Sect. D Biol. Crystallogr.* **54,** 905–921
29. Brunger, A. T., Adams, P. D., Clore, G. M., DeLano, W. L., Gros, P., Grosse-Kunstleve, R. W., Jiang, J. S., Kuszewski, J., Nilges, M., Pannu, N. S., Read, R. J., Rice, L. M., Simonson, T., and Warren, G. L. (1998) *Acta Crystallogr. D Biol. Crystallogr.* **54,** 905–921
30. Potterton, E., McNicholas, S., Krissinel, E., Cowtan, K., and Noble, M. (2002) *Acta Crystallogr. Sect. D Biol. Crystallogr.* **58,** 1955–1957
31. Kleywegt, G. J., and Jones, T. A. (1994) *Acta Crystallogr. Sect. D Biol. Crystallogr.* **50,** 178–185
32. Lawrence, M. C., and Colman, P. M. (1993) *J. Mol. Biol.* **234,** 946–950
33. Chesneau, V., and Rosner, M. (2000) *Protein Expression Purif.* **19,** 91–98
34. Zubarev, R. A. (2004) *Curr. Opin. Biotechnol.* **15,** 12–16
35. Zubarev, R. A., Kelleher, N. L., and McLafferty, F. W. (1998) *J. Am Chem.*

Soc. **120,** 3265–3266
36. Zubarev, R. A., Kruger, N. A., Fridriksson, E. K., Mark, L. A., Horn, D. M., Carpenter, B. K., and McLafferty, F. W. (1999) *J. Am Chem. Soc.* **121,** 2857–2862
37. Uggerud, E. (2004) *Int. J. Mass Spectrom.* **234,** 45–50
38. Page, J. S., Masselon, C. D., and Smith, R. D. (2004) *Curr. Opin. Biotechnol.* **15,** 3–11
39. Derewenda, U., Derewenda, Z., Dodson, E. J., Dodson, G. G., Reynolds, C. D., Smith, G. D., Sparks, C., and Swenson, D. (1989) *Nature* **338,** 594–596
40. Olsen, H. B., Ludvigsen, S., and Kaarsholm, N. C. (1996) *Biochemistry* **35,** 8836–8845
41. Huang, K., Chan, S. J., Hua, Q. X., Chu, Y. C., Wang, R. Y., Klaproth, B., Jia, W., Whittaker, J., De Meyts, P., Nakagawa, S. H., Steiner, D. F., Katsoyannis, P. G., and Weiss, M. A. (2007) *J. Biol. Chem.* **282,** 35337–35349
42. McKern, N. M., Lawrence, M. C., Streltsov, V. A., Lou, M. Z., Adams, T. E., Lovrecz, G. O., Elleman, T. C., Richards, K. M., Bentley, J. D., Pilling, P. A., Hoyne, P. A., Cartledge, K. A., Pham, T. M., Lewis, J. L., Sankovich, S. E., Stoichevska, V., Da Silva, E., Robinson, C. P., Frenkel, M. J., Sparrow, L. G., Fernley, R. T., Epa, V. C., and Ward, C. W. (2006) *Nature* **443,** 218–221
43. Ward, C. W., Lawrence, M. C., Streltsov, V. A., Adams, T. E., and McKern, N. M. (2007) *Trends Biochem. Sci.* **32,** 129–137
44. Glendorf, T., Sorensen, A. R., Nishimura, E., Pettersson, I., and Kjeldsen, T. (2008) *Biochemistry* **47,** 4743–4751
45. Kristensen, C., Kjeldsen, T., Wiberg, F. C., Schaffer, L., Hach, M., Havelund, S., Bass, J., Steiner, D. F., and Andersen, A. S. (1997) *J. Biol. Chem.* **272,** 12978–12983
46. Mayer, J. P., Zhang, F., and DiMarchi, R. D. (2007) *Biopolymers* **88,** 687–713
47. Udgaonkar, J. B. (2008) *Annu. Rev. Biophys.* **37,** 489–510
48. Xu, B., Hua, Q. X., Nakagawa, S. H., Jia, W., Chu, Y. C., Katsoyannis, P. G., and Weiss, M. A. (2002) *Protein Sci.* **11,** 104–116
49. DeMattos, R. B., Bales, K. R., Cummins, D. J., Paul, S. M., and Holtzman, D. M. (2002) *Science* **295,** 2264–2267
50. Nicoll, J. A., Wilkinson, D., Holmes, C., Steart, P., Markham, H., and Weller, R. O. (2003) *Nat. Med.* **9,** 448–452
51. Baker, N. A., Sept, D., Joseph, S., Holst, M. J., and McCammon, J. A. (2001) *Proc. Natl. Acad. Sci. U. S. A.* **98,** 10037–10041